

A study of Channeling, Volume Reflection and Volume Capture of 3.35 - 14.0 GeV Electrons in a bent Silicon Crystal

T.N. Wistisen and U.I. Uggerhøj

Department of Physics and Astronomy, Aarhus University, 8000 Aarhus, Denmark

U. Wienands, T.W. Markiewicz, R.J. Noble, B.L. Benson and T. Smith

SLAC National Accelerator Laboratory, 2575 Sand Hill Road, Menlo Park, California 94025

E. Bagli, L. Bandiera, G. Germogli, V. Guidi and A. Mazzolari

Department of Physics and Earth Sciences of the University of Ferrara, and INFN Section of Ferrara, Via Saragat 1/C, I-44122 Ferrara, Italy

R. Holtzapple and S. Tucker

California Polytechnic State University, San Luis Obispo, California 93407, USA

Abstract

We present the experimental data and analysis of experiments conducted at SLAC National Accelerator Laboratory investigating the processes of channeling, volume-reflection and volume-capture along the (111) plane in a strongly bent quasi-mosaic silicon crystal. These phenomena were investigated at 5 energies: 3.35, 4.2, 6.3, 10.5 and 14.0 GeV with a crystal with bending radius of 0.15m, corresponding to curvatures of 0.070, 0.088, 0.13, 0.22 and 0.29 times the critical curvature respectively. Based on the parameters of fitting functions we have extracted important parameters describing the channeling process such as the dechanneling length, the angle of volume reflection, the surface transmission and the widths of the distribution of channeled particles parallel and orthogonal to the plane.

1. Introduction

Channeling in bent crystals has been thoroughly studied for protons with the purpose of e.g. proton extraction at accelerator facilities [1], [2], [3]. Much less is known about the efficiency of channeling of electrons in bent crystals. In this paper we present a quantitative investigation of channeling and related phenomena in a strongly bent Silicon crystal. The ordered structure of the crystal lattice gives a unique access to electromagnetic field strengths otherwise experimentally inaccessible [4] which can be manipulated by e.g. bending of the crystal, as in this experiment, or otherwise inducing a strain in the crystal as exploited in certain new types of crystalline undulators [5], [6], [7]. Understanding the dynamics of the electron motion in a bent crystal is important both for the application of bent crystals,

but also in order to obtain a better understanding of the dynamics in e.g. crystalline undulators. This paper is a continuation of [8]. Here we include experiments at three other energies conducted after the submission of [8], thus presenting a far more detailed study.

2. Theory

Channeling is a phenomenon which occurs in aligned single crystals. If an impinging particle is traveling along a direction of symmetry in the crystal, the motion will no longer be governed by the particle's interaction with an individual atom, but the coherent interaction of many atoms along a crystalline axis or plane. This allows one to average the potential of each atom over the general direction of motion (along the axis or plane), yield-

ing the 'continuum' transverse potential. An often employed model of the planar (111) continuum potential is the thermally averaged Doyle-Turner potential of the form [9]

$$U(x) = 2\sqrt{\pi}Z_1 \frac{e^2}{a_0} a_0^2 N d_p \sum_{i=1}^4 \frac{a_i}{\sqrt{B_i + \rho^2}} e^{-\frac{x^2}{B_i + \rho^2}}, \quad (1)$$

where Z_1 is the charge number of the projectile, $\rho = 0.062 \text{ \AA}$ is the r.m.s. thermal vibrational amplitude at room temperature for Si, $a_0 = 0.53 \text{ \AA}$ is the Bohr radius, N is the number density of atoms and $B_i = b_i/4\pi^2$. See 1 for the values of a_i and b_i . A plot of this potential versus transverse position is shown in 1. For Si (111) there are two planar distances given by $d_1 = \frac{a}{4\sqrt{3}}$ and $d_2 = \frac{a\sqrt{3}}{4}$ with $a = 5.43 \text{ \AA}$ being the lattice constant for Si and $d_p = \frac{d_1+d_2}{2}$. For Si the coefficients are given by [10]:

i	1	2	3	4
$a_i[\text{\AA}]$	2.1293	2.533	0.8349	0.3216
$b_i[\text{\AA}^2]$	57.7748	16.4756	2.8796	0.3860

Table 1: A table of parameters for the Doyle-Turner potential for the Si potential of 1.

The potential 1 depends only on one coordinate, transverse to the (111) plane. We define the 'transverse mechanical energy' as

$$E_\perp = \frac{p_\perp^2}{2\gamma m} + U(x), \quad (2)$$

which is a conserved quantity to leading order in $\frac{1}{\gamma^2}$. Here p_\perp is the momentum component normal to the plane and γ is the relativistic Lorentz factor of the impinging electron. The critical angle is defined as the largest angle the electron can have with the plane while still being bound in the transverse potential. From 2 one obtains

$$\theta_c = \frac{p_{\perp,\max}}{p} = \sqrt{\frac{2U_0}{E\beta^2}}, \quad (3)$$

where U_0 is the depth of the potential, E the energy of the impinging electron and $\beta = \frac{v}{c}$ its velocity in units of c , the speed of light. In a bent crystal channeling is easily described in a rotating

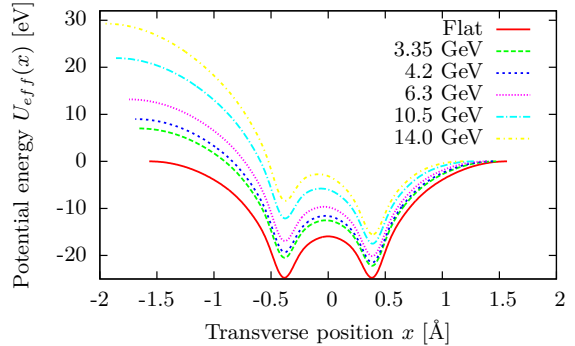


Figure 1: A plot of the effective potential of 5 for a flat crystal and for the relevant electron energies with bending radius $R = 0.15 \text{ m}$.

coordinate system such that the x-coordinate is the displacement from the bent channel in the radial direction of the bending arc. This choice of coordinate system gives rise to a centrifugal force. For a relativistic particle this is equivalent to a centrifugal barrier potential of the form

$$U_{\text{CF}}(x) = \frac{Ex}{R}, \quad (4)$$

where x is the displacement from the center of the channel and R the bending radius of the crystal. The motion of the channeled particle is therefore described by an effective potential

$$U_{\text{eff}}(x) = U(x) + \frac{Ex}{R}. \quad (5)$$

See 1 for plots of the potential for the relevant energies. It is evident that the bending of the crystal reduces the potential depth and thus the critical angle in 3. If the centrifugal potential barrier of 4 changes by a significant amount compared to the potential depth of the unbent crystal over an inter planar distance one approaches criticality, and the bending of the crystal can not be treated as a small perturbation to the unbent case. This condition can also be written as

$$R_{\text{crit}} = \frac{Ed_p}{2U_0}. \quad (6)$$

For the case of protons this corresponds to the Tsyanov critical radius of bending. From 4 it is seen that when $U_0 \simeq 25 \text{ eV}$, $d_p = 1.57 \text{ \AA}$, the critical radius for 14.0 GeV is 4.4 cm which is comparable to the 15 cm radius of curvature of the crystal in this experiment.

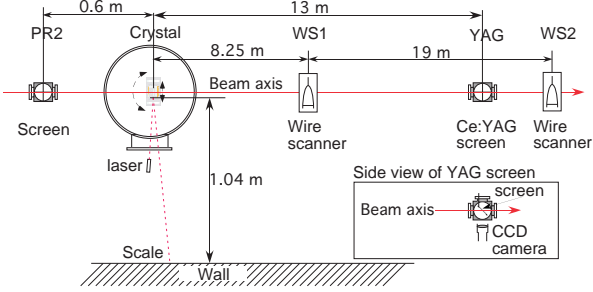


Figure 2: A sketch of the experimental setup.

Dechanneling

In a crystal of significant length, the simple picture of a conserved transverse mechanical energy is too simple. Multiple scattering of the channeled particle leads to an increasing transverse mechanical energy that results in the particle leaving the channel and the motion is no longer bound. The typical length over which this happens is called the dechanneling length and its size is found by equating the scattering angle due to multiple scattering to the critical angle of 3. The result is given by [11]

$$L_d = \frac{\alpha U_0 E}{\pi m^2} X_0, \quad (7)$$

where α is the fine structure constant and X_0 the radiation length in the amorphous medium. A simple model of dechanneling is obtained by assuming a constant probability per unit length per particle to dechannel, $\frac{1}{L_d}$, giving an exponential decay of the number of particles in the channel [12], [13],

$$N(z) = N_0 e^{-\frac{z}{L_d}}. \quad (8)$$

8 is for the dechanneling length in a straight crystal. For positively charged particles most of the particles will populate the low lying states and 7 is quite accurate. However for negatively charged particles, the large majority of particles are weakly bound, such that using the potential depth U_0 as the typical initial transverse mechanical energy is inaccurate. This simple model can easily be modified to the case of a bent crystal. From 5 it is seen that the potential depth from the case of a straight crystal is, to first order in $\frac{1}{R}$, reduced by $\frac{Ed_p}{2R} = \frac{R_{\text{crit}}}{R} U_0$ such that the dechanneling length is instead given by

$$L_d = \frac{\alpha U_0 E}{\pi m^2} X_0 \left(1 - \frac{R_{\text{crit}}}{R} \right), \quad (9)$$

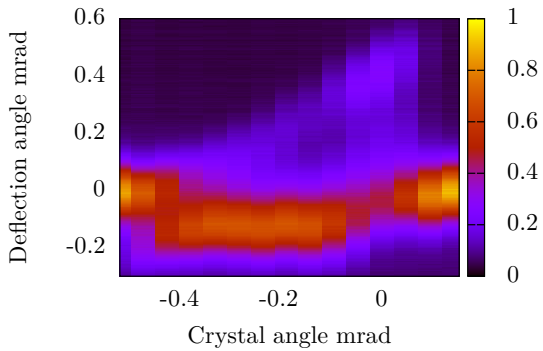


Figure 3: The probability density relative to the maximum probability density of the deflected particles as a function of the crystal angle for the case of 3.35 GeV electrons.

which is accurate while R is significantly larger than R_{crit} .

Volume capture and volume reflection

The phenomenon of volume capture [14] in a bent crystal is the process where a particle, initially unbound, scatters and loses transverse mechanical energy to become bound - 'captured' in the channel. As such it is closely related to the dechanneling phenomenon [15]. Volume capture occurs when the particle is not aimed directly into the acceptance of the channel, but at an angle less than the total bending of the crystal. A rudimentary model of the volume capture efficiency can be obtained in the following manner. An incoming particle is close to the barrier over a distance on the order of $\theta_c R$ and since multiple scattering will randomly increase or decrease the transverse mechanical energy the probability per unit length per particle to become captured is also $\frac{1}{L_d}$ and therefore the volume capture efficiency should scale as $\frac{\theta_c R}{L_d}$ which gives an energy dependence of $E^{-\frac{3}{2}}$, assuming 7 to be correct. Particles not captured in this manner will remain unbound, but will be deflected with respect to the incoming beam in a direction opposite to the captured particles. This effect is known as volume reflection [16]. In 5 there is an additional linear term in the potential as compared to the case of a straight crystal which means a volume reflected particle initially starts with transverse mechanical energy far above the potential barrier until reaching the turning point at which the crystal potential causes an additional deflection of at most the critical angle. Therefore one expects the angle of

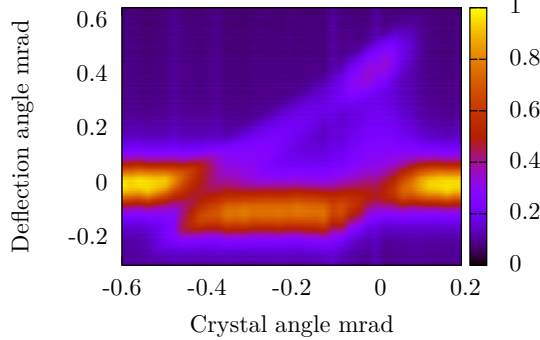


Figure 4: The probability density relative to the maximum probability density of the deflected particles as a function of the crystal angle for the case of 4.2 GeV electrons.

volume reflection to be similar to the critical angle i.e. with an energy dependence of $E^{-\frac{1}{2}}$.

Surface transmission

For a beam with no angular divergence, the surface transmission can be determined analytically. The surface transmission is defined as the fraction of particles that become transversely bound upon entry into the crystal to the total number of incoming particles. Over a single channel the distribution of incoming particles is uniform, therefore the surface transmission is the ratio of the length over which the potential seen in 1 is negative, compared to the length over which the force is periodic which is roughly $2d_p$. By approximating the potential in 1 by a parabola around the point $-d_p$, one can determine the surface transmission. Making the approximation that this potential is of the form $-(x - d_p)^2 \frac{U_0}{d_p^2}$ one obtains

$$A = \left(1 - \frac{2u}{d_p}\right) \left(1 - \frac{\sqrt{1 + \frac{4R}{R_c}}}{1 + \frac{2R}{R_c}}\right), \quad (10)$$

where $u = 0.062\text{\AA}$ is the thermal vibrational amplitude for Si at room temperature, and the front factor has been added to account for the immediate dechanneling due to thermal vibrations. The bending efficiency is defined as the fraction of incoming particles which make it to the end of the crystal and is expressed as

$$\varepsilon = Ae^{-\frac{L}{L_D}}. \quad (11)$$

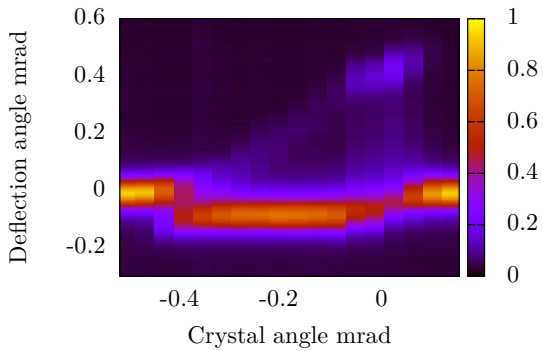


Figure 5: The probability density relative to the maximum probability density of the deflected particles as a function of the crystal angle for the case of 6.3 GeV electrons.

Simulations

We will compare the experimental measurements with the simulation code DYNECHARM++ [17]. The code allows the tracking of a relativistic charged particle inside a crystalline medium via the numerical integration of the classical equations of motion. The continuum potential approximation proposed by Lindhard is used [18]. The electrical characteristics of the crystal within this approximation are computed by means of the ECHARM code [19]. Since the multiple and single scatterings may cause the particle to dechannel/rechannel, such incoherent scattering has been included into the simulation. Since the encountered number of nuclei and electrons depends from the particle trajectory [18], in the simulation the normalized distribution of scattering angles [20] scales with the ratio between the density of matter encountered by a particle and the average density of the material. Moreover, the experimental measurements were compared with the results of the Geant4 Monte Carlo toolkit [21], which allows the simulation of the coherent effects of charged particles in crystals [22].

3. Experimental setup and procedure

The silicon (Si) crystal used in this experiment was fabricated [23] at the Sensors and Semiconductor Laboratory at the University of Ferrara with crystallographic orientation chosen to produce quasi-mosaic bending of the (111) plane [24]. Its thickness was measured interferometrically to be $60 \pm 1 \mu\text{m}$. The (111) plane has a bending radius of 0.15 m giving a total bending angle of the crystal of $\theta_b = 402 \pm 9 \mu\text{rad}$ in the horizontal direction.

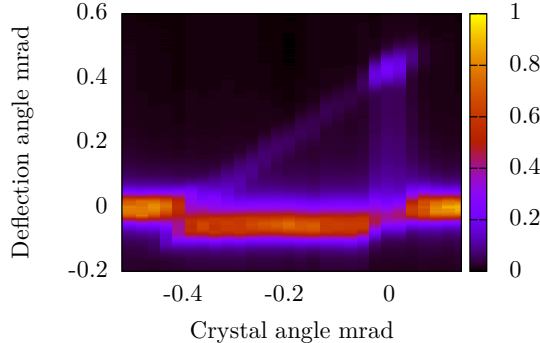


Figure 6: The probability density relative to the maximum probability density of the deflected particles as a function of the crystal angle for the case of 10.5 GeV electrons.

The crystal was mounted in a scattering chamber in the End Station A Test Beam at SLAC, see 2. A rotational stage allows rotation of the crystal with step sizes of approximately 10 μ rad. A translational stage moves the crystal to its optimal position. The rotation angle of the crystal is determined by reflecting a laser beam off a flat mirror mounted on the side of the crystal holder. The reflected laser beam hits a screen approximately 1m from the mirror. When the crystal is rotated, the laser beam on the screen provides a read-out of the rotation angle of the crystal with a resolution better than 5 μ rad. A Cerium doped Yttrium Aluminum Garnet (YAG for short) screen of 500 μ m thickness with a CCD camera 13 m down stream of the crystal provides the means of data acquisition in this experiment. Saturation of the YAG screen is negligible at the bunch charge 10^8 particles per bunch that was provided for this experiment [25]. The beam divergence was measured to be less than 10 μ rad by the wire scanners. The spot-size was less than 150 μ m and the momentum spread reduced to about 0.15%.

4. Data analysis and results

The experimental measurements were performed by rotating the crystal in small angular steps and recording an image of the circular YAG screen. The camera was mounted at an angle with respect to the screen which distorted the image. An ellipse was fitted along the edge of the screen, for this was known to be circular. This allows one to revert this image distortion due to the positioning of the camera. A region of the screen is chosen such that the edge of the screen is avoided. The crystal deflects particles

in the horizontal plane and we sum the intensity in the vertical plane and normalize the probability distribution as seen in e.g. 7. For each crystal angle several images were taken. Images with low or high (camera saturated) light intensities were ignored. Plotting the distribution along the y-axis with the crystal angle along the x-axis one obtains the so called 'triangle plots', (3 to 6 represent the raw data). A crystal angle of 0 was chosen to be the orientation of closest direct entry of the beam into the channel as could be experimentally realized. This orientation, along with the halfway of the full bending of $\theta_b = 402 \mu$ rad, (roughly $\frac{\theta_b}{2}$) termed the volume reflection orientation, will be investigated in detail.

In 7 and 8 the probability density of the deflected particles is plotted for the two different cases described above. In 7, some general tendencies can be identified. The width of the large leftmost peak, becomes narrower as does the channeled peak due to the decreasing critical angle. In 8 the large leftmost peak due to volume reflection moves closer to the undeflected position and the width decreases as energy increases. To extract quantitative information from these distributions we consider a fitting procedure consisting of two Gaussian probability distributions for the two peaks and a function for the dechanneled particles in between to be specified. For $i = 1, 2$ we have two Gaussian distributions

$$\frac{dP}{d\theta} = \frac{P_i}{\sigma_i \sqrt{2\pi}} e^{-\frac{(x-\mu_i)^2}{2\sigma_i^2}}, \quad (12)$$

where P_i is the fraction of particles in this peak, σ_i the standard deviation of the distribution and μ_i the center. The undeflected/volume reflected particles are denoted by $i = 1$ and either the channeled or volume captured particles are denoted by $i = 2$. The probability to dechannel per angle in the exponential decay model of 8 is $\frac{dP}{d\theta} = e^{-\frac{\theta}{\theta_d}} / \theta_d$. Therefore the probability distribution of the dechanneled particles becomes

$$\frac{dP}{d\theta}(\theta) = \int_{\mu_1}^{\mu_2} \frac{1 - P_1}{\sigma_2 \sqrt{2\pi}} e^{-\frac{(\theta-\theta')^2}{2\sigma_2^2}} \frac{1}{\theta_d} e^{-\frac{\theta'}{\theta_d}} d\theta', \quad (13)$$

where $\theta_d = \frac{L_d}{L} \theta_b$. This formula can be understood as follows: The probability to find a particle at an angle θ is the sum over the possible ways this can happen. A fraction of the particles dechanneling at angle θ' can end up at the angle θ due to the

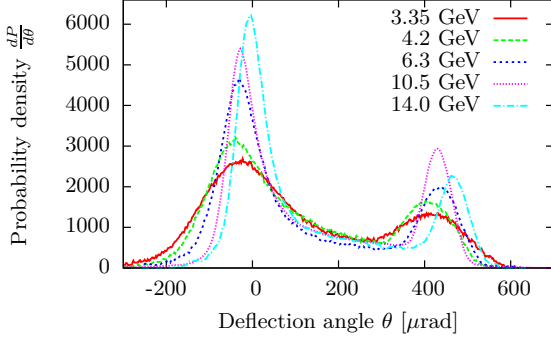


Figure 7: The probability density of the deflected particles when the crystal is in the channeling orientation for the different energies in the experiment.

distribution of particles in the channel. The above can also be rewritten as

$$\frac{dP}{d\theta}(\theta) = \frac{1 - P_1}{2\theta_d} e^{\frac{\sigma_2^2}{2\theta_d^2} + \frac{\mu_1}{\theta_d} - \frac{\theta}{\theta_d}} \times \left(\operatorname{erf} \left(\frac{\mu_2 - \Delta\theta}{\sqrt{2}\sigma_2} \right) - \operatorname{erf} \left(\frac{\mu_1 - \Delta\theta}{\sqrt{2}\sigma_2} \right) \right), \quad (14)$$

where $\Delta\theta = \theta - \frac{\sigma_2^2}{\theta_d}$. The exponential dechanneling model means that P_2 is given by $P_2 = (1 - P_1)e^{-\frac{L}{L_d}}$. This model therefore contains six free parameters: P_1 , σ_1 , μ_1 , σ_2 , μ_2 , L_d . It turns out that the non-Gaussian tail of the undeflected peak has a large influence on the fit between the two peak functions which is important when trying to determine the dechanneling length. A sum of two Gaussians fits the peak in the 'amorphous' orientation very well which we write in the form

$$\frac{dP}{d\theta} = P_1 \left(\frac{A}{\sigma_1 \sqrt{2\pi}} e^{-\frac{(x-\mu_1)^2}{2\sigma_1^2}} + \frac{1-A}{r\sigma_1 \sqrt{2\pi}} e^{-\frac{(x-\mu_1)^2}{2r^2\sigma_1^2}} \right), \quad (15)$$

where the standard deviation of the second Gaussian is $r\sigma_1$. The values of A and r were then found by performing a fit in the 'amorphous' orientation and we obtain the following values:

E [GeV]	3.35	4.2	6.3	10.5	14.0
A	0.571	0.776	0.872	0.696	0.77
r	1.52	2.19	2.04	2.27	3.10

Table 2: A table of the fitting parameters used to describe the distribution in the 'amorphous' orientation.

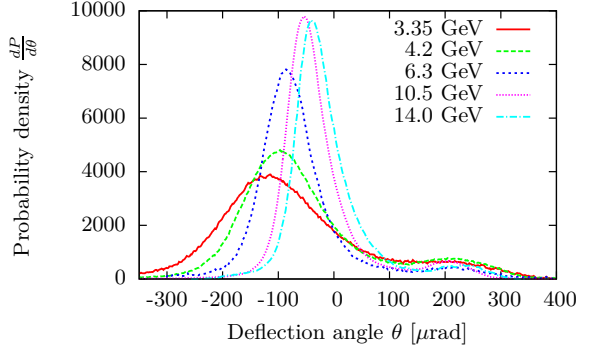


Figure 8: The probability density of the deflected particles when the crystal is at half of the full bending angle. The large leftmost peaks are the volume reflected portions and the small rightmost peaks are the volume captured particles.

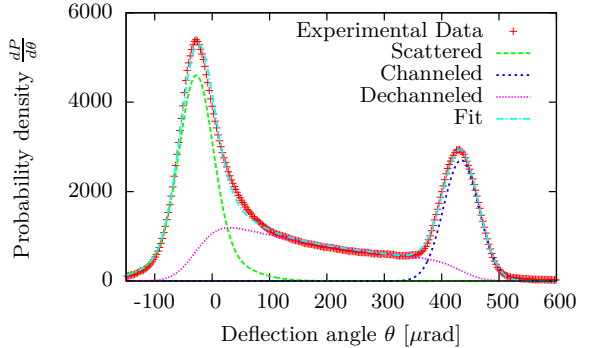


Figure 9: A fit to the 10.5 GeV experimental data in the channeling orientation.

In 9 and 10 the data in the 'channeling' orientation for the lowest and a high energy are fitted according to the model described here. The results are shown in 3.

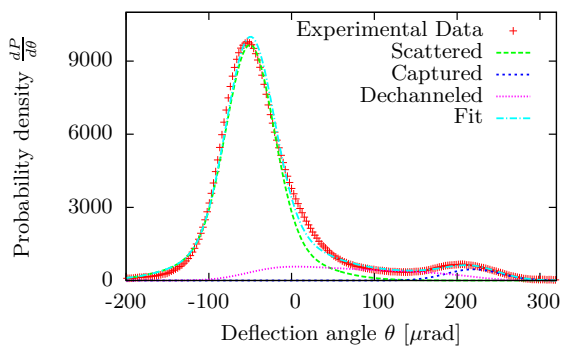


Figure 11: A fit to the 10.5 GeV experimental data at half the crystal bending angle.

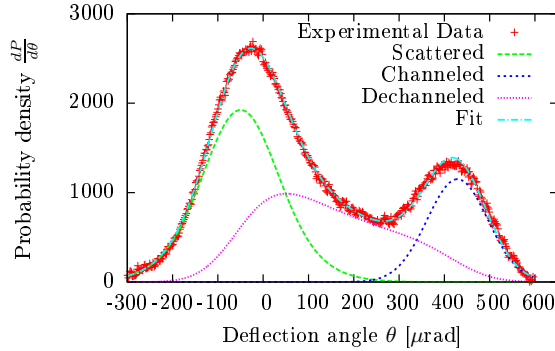


Figure 10: A fit to the 3.5GeV experimental data in the channeling orientation.

E [GeV]	3.35	4.2	6.3	10.5	14.0
L_d [μm]	55.4 ± 1.8	45.2 ± 1.2	65.3 ± 1.9	57.5 ± 1.2	55.8 ± 1.2
P_1 [%]	43 ± 1.3	33 ± 1.5	50 ± 0.8	41 ± 0.7	49 ± 0.7
μ_1 [μrad]	-49.9 ± 2.3	-62.4 ± 2.3	-33.8 ± 1.0	-28.4 ± 0.8	0.29 ± 0.5
μ_2 [μrad]	428.8 ± 1.45	419.8 ± 1.5	439.2 ± 1.2	433.9 ± 0.8	470.3 ± 0.9
σ_1 [μrad]	76.1 ± 0.92	53.9 ± 1.1	49.2 ± 0.8	29.0 ± 0.5	29.0 ± 0.5
σ_2 [μrad]	67.0 ± 1.1	48.5 ± 1.0	42.6 ± 0.9	30.9 ± 0.6	34.1 ± 0.7

Table 3: A table of the fitting parameters for the crystal in 'channeling' orientation using the described model.

E [GeV]	3.35	4.2	6.3	10.5	14.0
L_d [μm]	39.4 ± 0.3	47.4 ± 0.5	54.3 ± 0.5	57.1 ± 0.6	48.1 ± 0.8
P_1 [%]	11 ± 0.9	27 ± 0.7	34 ± 0.4	38 ± 0.3	40.1 ± 0.6
μ_1 [μrad]	-97.6 ± 2.1	-57.0 ± 2.3	-37.5 ± 0.5	-25.5 ± 0.3	-20.6 ± 0.4
μ_2 [μrad]	441.4 ± 0.5	439.2 ± 0.5	438.7 ± 0.3	437.6 ± 0.3	437.4 ± 0.5
σ_1 [μrad]	78.1 ± 3.6	56.0 ± 0.9	39.4 ± 0.3	24.8 ± 0.2	16.8 ± 0.3
σ_2 [μrad]	50.4 ± 0.7	42.8 ± 0.6	31.9 ± 0.2	21.5 ± 0.2	17.4 ± 0.3

Table 4: A table of the fitting parameters for the crystal DYNECHARM simulation in 'channeling' orientation using the described model.

E [GeV]	3.35	4.2	6.3	10.5	14.0
L_d [μm]	35.5 ± 3.9	45.6 ± 3.1	36.4 ± 3.8	40.9 ± 3.4	25.6 ± 3.7
P_1 [%]	67 ± 3.8	73 ± 1.3	84 ± 1.1	84 ± 0.9	80.7 ± 2.3
μ_1 [μrad]	-128.8 ± 4.1	-100.7 ± 1.2	-84.0 ± 0.9	-50.3 ± 0.6	-35.6 ± 1.4
μ_2 [μrad]	242.1 ± 5.3	239.9 ± 3.6	243.3 ± 8.1	219.8 ± 3.7	258.0 ± 9.5
σ_1 [μrad]	73.5 ± 1.2	58.1 ± 0.7	42.8 ± 0.7	28.5 ± 0.4	28.2 ± 0.9
σ_2 [μrad]	57.9 ± 3.0	55.8 ± 2.3	55.0 ± 5.6	32.9 ± 2.6	27.0 ± 6.1

Table 5: A table of the fitting parameters for the crystal in 'volume capture' orientation using the described model.

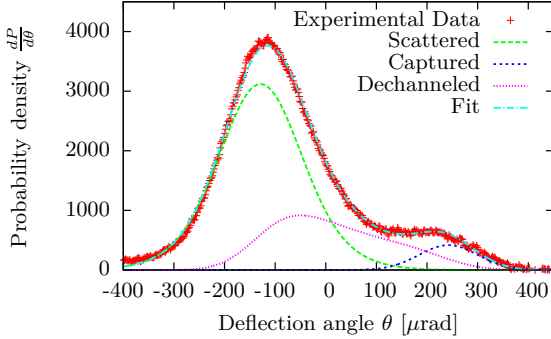


Figure 12: A fit to the 3.5 GeV experimental data at half the crystal bending angle.

Performing the same type of fit to the results of the simulations shown in 13 one obtains the results shown in 4.

The errors given here are only statistical. The simulations were performed with beam angular divergences of 30μrad, 27.5μrad, 21.5μrad, 10μrad and 10μrad for the energies 3.35GeV, 4.2GeV, 6.3GeV, 10.5GeV and 14.0GeV respectively.

Similarly in 11 and 12, the same fit is applied to the case where the crystal is roughly at the angle of $\frac{\theta_b}{2}$ and the results are shown in 5.

It is important to note that the model presented here is different than the one used for the analysis of the 3.35 and 6.3GeV data seen in [8]. Therefore different numbers for e.g. the dechanneling length is obtained. In particular the approach using a double gaussian for the amorphous/VR peak is a difference and that we in the model used in this paper have one less fitting parameter. This model is thus more constrained. In [8] it was noted that the dechanneling length could be determined in two ways. One based on the shape of the distribution (e.g. 10) between the two peaks, and another based on the relative sizes of the two peaks. In [8] this gave rise to two different dechanneling lengths. The model used here is constrained such that this is not a possibility. Using one less fitting parameter it is expected that the fit could be worse. However, generally the fits are good, but worse for higher energy than at low energies (10.5 and 14GeV are about equally good). Only in the case of the VR orientation at 14GeV is the fit worse than the example shown by 11 but this also to a considerable degree.

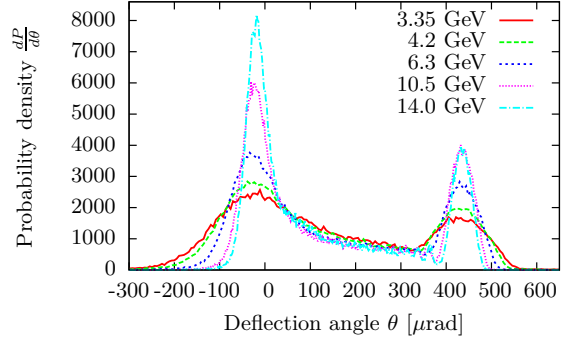


Figure 13: The probability density of the deflected particles obtained from the DYNECHARM simulation when the crystal is in the channeling orientation for the different energies in the experiment.

4.1. Multiple scattering of channeled particles parallel to the plane

In 14 we have plotted the r.m.s. standard deviation, σ_{\parallel} , of the Gaussian function fitted to the distribution of channeled particles in the direction parallel to the plane i.e. in the 'free' direction in the continuum potential approximation. It is therefore expected that multiple scattering determines the width in this case. The multiple scattering width scales as $1/E$ and performing a fit we obtain the best fit to be given by

$$\sigma_{\parallel} = \frac{520\mu\text{rad} \times \text{GeV}}{E}. \quad (16)$$

The usual formula [26] for multiple scattering would predict the factor to be 302μrad × GeV, thus an increased scattering is observed. This is likely due to negative particles crossing the plane during channeling oscillations and thus more often encounter hard scattering with the nuclei [27], [12], [28].

4.2. Angular distribution of channeled particle orthogonal to the plane

In 15 we have plotted the r.m.s. standard deviations σ_2 from 3 and a fit to a power function that yields

$$\sigma_2 = 117\mu\text{rad} \times E[\text{GeV}]^{-0.53}. \quad (17)$$

Since the critical angle scales as $1/\sqrt{E}$ we have also performed such a fit to obtain

$$\sigma_2 = 111\mu\text{rad} \times E[\text{GeV}]^{-0.5}. \quad (18)$$

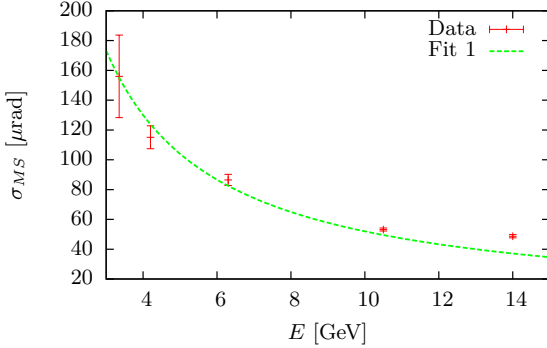


Figure 14: The width of the channeling peak in the direction parallel to the plane is fitted to obtain 16.

4.3. Deflection angle of volume reflected particles

In 16 we have plotted the deflection angle in volume capture orientation ($-\mu_1$ from 5) versus the beam energy and fit the data to two different functions. Fitting the data to a power function we obtain

$$|\mu_1| = 338 \mu\text{rad} \times E[\text{GeV}]^{-0.81}. \quad (19)$$

Again, we would expect there to be a $1/\sqrt{E}$ scaling. With such a fit we obtain

$$|\mu_1| = 207 \mu\text{rad} \times E[\text{GeV}]^{-0.5}. \quad (20)$$

4.4. Efficiency of volume capture

In the case of 'volume reflection orientation', P_1 gives the fraction of reflected particles and the rest will have been captured, such that $1 - P_1$ is the fraction of particles captured. From 2, we expect the volume reflection to scale with energy as $E^{-3/2}$ [15]. We have therefore performed such a fit along with a fit to a power function, see 19, and obtained

$$\varepsilon_{\text{VR}} = 2.3 \times E[\text{GeV}]^{-1.5}, \quad (21)$$

and

$$\varepsilon_{\text{VR}} = 0.57 \times E[\text{GeV}]^{-0.52}. \quad (22)$$

It is seen that the fitted power function is close to a $1/\sqrt{E}$ scaling. If one assumes an energy independent dechanneling length L_D as is indicated experimentally, one would also expect the volume capture efficiency to instead scale as $1/\sqrt{E}$. Although this observation may be surprising, the data set thus consistently shows a dechanneling length that is largely independent on energy.

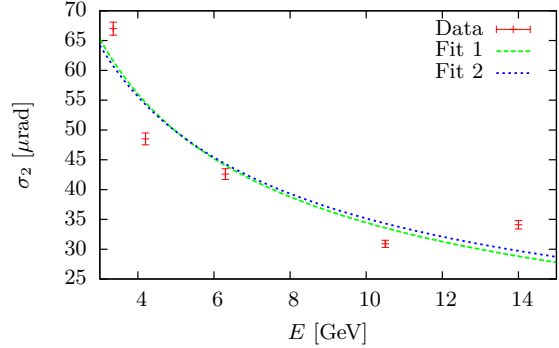


Figure 15: The width of the channeling peak in the direction orthogonal to the plane is fitted with a power function (Fit 1), see 17 and to a function of the type a/\sqrt{E} (Fit 2), see 18.

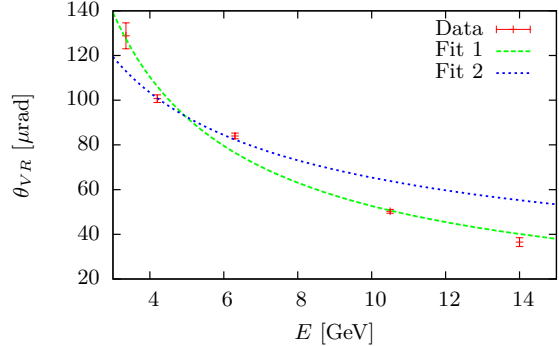


Figure 16: The angle of volume reflection is fitted with a power function (Fit 1) and to a function of the type a/\sqrt{E} (Fit 2).

4.5. Discussion of the dechanneling length and surface transmission

In 4 and 17 it is evident that the dechanneling lengths obtained from the simulation has a dependence on energy which is not proportional as the simple formula of 7 prescribes. The main reasons for this discrepancy is the influence of the bending of the crystal and the beam angular divergence. The angular divergence of the beam determines the distribution of the transverse mechanical energy of the captured particles and the dynamics of dechanneling depends on this. Likewise, the beam entry angle plays an important role in the dechanneling length of the captured particles. This can be observed in the experimental data because the dechanneling lengths obtained in the 'VR orientation', as shown in 5, are consistently lower than in the 'channeling orientation' shown in 3. Whereas in the simulations, the beam entered directly into

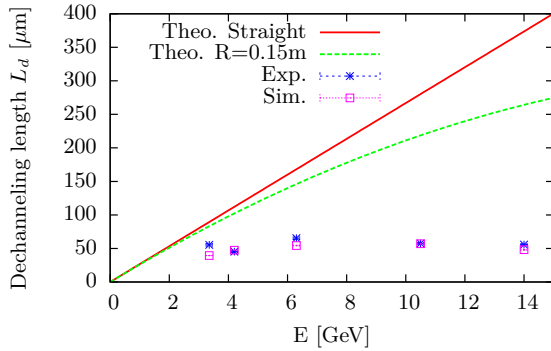


Figure 17: A plot of the 'simple' dechanneling formulas of 7, 9 and of the experimental and simulated values.

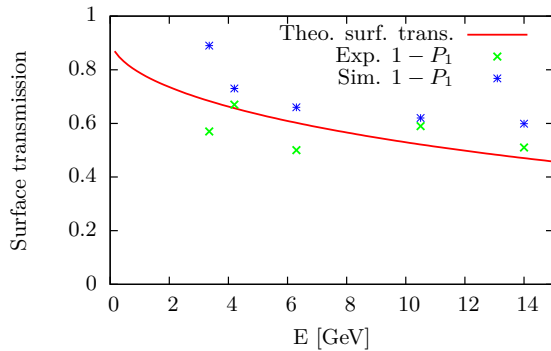


Figure 18: The experimental and simulated values of the surface transmission given by $1 - P_1$ is compared with the model of 10.

the channel. In the experiment however, the angular resolution of the rotational stage means that this orientation cannot be determined more accurately than this. 7 shows that the angular position of the 'channeling peak' varies slightly in contrast to the simulations seen in 13, which supports this hypothesis. We deem this the most likely reason for the discrepancies seen between the values of the dechanneling lengths in the experiment versus simulation shown in 3 and 4. It is also clear from 17 that the dechanneling length is significantly shorter than predicted by 7 which must be a general property of channeling of negatively charged particles.

The measured and calculated (from 10) values of the surface transmission are in good agreement and are plotted in 18. In this case the fluctuation of the data points around this curve we also attribute to the uncertainty on the beam entry angle.

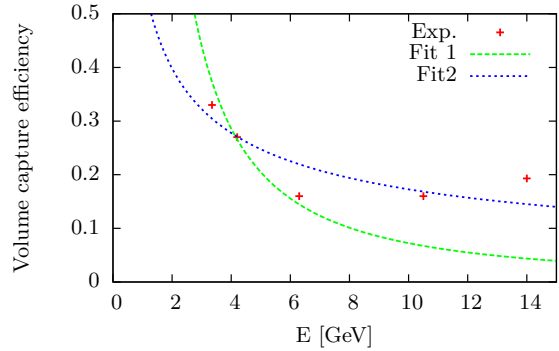


Figure 19: The volume capture efficiency as given by $1 - P_1$ from 5. 'Fit 1' is a fit to a function of the type $aE^{-3/2}$ and 'Fit 2' is a fit to a power function (aE^b).

5. Conclusion

We have shown that a fitting procedure based on 1) a simple exponential decay model of channeled particles and 2) that these particles are distributed according to a Gaussian distribution within the channel, fit the data with good agreement. Based on the parameters of the fitting functions we have extracted important parameters describing the channeling process such as the dechanneling length, the angle of volume reflection, the surface transmission and the widths of the distribution of channeled particles parallel and orthogonal to the plane. The scattering parallel to the plane fits well with the usual functional dependence of multiple scattering on energy but is larger than amorphous/random by a factor of 1.7. For the distribution of channeled particles, the mean of the angle of volume reflection and the efficiency of volume capture, were fit to power functions with a free exponent and to a exponent fixed by that predicted by 'simple' theory. In these cases, a significant deviation is seen in the exponent which indicates that the 'simple' theory may be too simple to describe the results of this experiment. The 'simple' formula for surface transmission, however, works out well. The dechanneling lengths observed in these experiments are significantly shorter than predicted by the 'simple' theory and the dechanneling length in 'VR orientation' is seen to be consistently smaller than in 'channeling orientation'. However, in the DYNECHARM simulation, good agreement is seen in the angular distributions of the exiting particles and the obtained dechanneling lengths.

This work was partially supported by the U.S. DOE under Contract No. DE- AC02-76SF00515,

by the U.S. National Science Foundation (Grant No. PHY-1068662), by the Danish Council for Independent Research — Natural Sciences FNU, and the Italian Istituto Nazionale di Fisica Nucleare (INFN) through the CHANNEL experiment. We wish to acknowledge also Mr. Persiani Andrea and Mr. Manfredi Claudio of Perman (Loiano, Italy) for their support with crystal holders manufacturing. Gilles Frequet from Fogale Nanotech for precise measurement of crystal thickness by means of a T-MAP IR interferometer.

[1] W. Scandale, A. Carnera, G. Della Mea, D. De Salvador, R. Milan, A. Vomiero, S. Baricordi, P. Dalpiaz, M. Fiorini, V. Guidi, G. Martinelli, A. Mazzolari, E. Milan, G. Ambrosi, P. Azzarello, R. Battiston, B. Bertucci, W. J. Burger, M. Ionica, P. Zuccon, G. Cavoto, R. Santacesaria, P. Valente, E. Vallazza, A. G. Afonin, V. T. Baranov, Y. A. Chesnokov, V. I. Kotov, V. A. Maisheev, I. A. Yazynin, S. V. Afanasiev, A. D. Kovalenko, A. M. Taratin, A. S. Denisov, Y. A. Gavrikov, Y. M. Ivanov, V. G. Ivochkin, S. V. Kosyanenko, A. A. Petrunin, V. V. Skorobogatov, V. M. Suvorov, D. Bolognini, L. Foggetta, S. Hasan, and M. Prest, *Phys. Rev. ST Accel. Beams* **11**, 063501 (2008).

[2] R. A. Carrigan, D. Chen, G. Jackson, N. Mokhov, C. T. Murphy, S. Baker, A. Bogacz, D. Cline, S. Ramachandran, J. Rhoades, J. Rosenzweig, A. Asseev, V. Biryukov, A. Taratin, J. A. Ellison, A. Khanzadeev, T. Prokofieva, V. Samsonov, G. Solodov, B. Newberger, E. Tsyanov, H.-J. Shih, W. Gabella, B. Cox, V. Golovatyuk, and A. McManus, *Phys. Rev. ST Accel. Beams* **5**, 043501 (2002).

[3] S. MÄžller, E. UggerhÃžj, H. Atherton, M. ClÃ©ment, N. Doble, K. Elsener, L. Gatignon, P. GrafstrÃ¶m, M. Hage-Ali, and P. Siffert, *Physics Letters B* **256**, 91 (1991).

[4] U. I. Uggerhøj, *Rev. Mod. Phys.* **77**, 1131 (2005).

[5] T. N. Wistisen, K. K. Andersen, S. Yilmaz, R. Mikkelsen, J. L. Hansen, U. I. Uggerhøj, W. Lauth, and H. Backe, *Phys. Rev. Lett.* **112**, 254801 (2014).

[6] Nuclear Instruments and Methods in Physics Research Section B: Beam Interactions with Materials and Atoms **309**, 45 (2013), the 5th International Conference.

[7] U. Mikkelsen and E. UggerhÃžj, Nuclear Instruments and Methods in Physics Research Section B: Beam Interactions with Materials and Atoms **160**, 435 (2000).

[8] U. Wienands, T. W. Markiewicz, J. Nelson, R. J. Noble, J. L. Turner, U. I. Uggerhøj, T. N. Wistisen, E. Bagli, L. Bandiera, G. Germogli, V. Guidi, A. Mazzolari, R. Holtzapple, and M. Miller, *Phys. Rev. Lett.* **114**, 074801 (2015).

[9] S. P. Møller, Nuclear Instruments and Methods in Physics Research Section A: Accelerators, Spectrometers, Detectors and Associated Equipment **361**, 403 (1995).

[10] S. Møller, (1995).

[11] V. Baier, V. Katkov, and V. Strakhovenko, *Electromagnetic Processes at High Energies in Oriented Single Crystals* (World Scientific, 1998).

[12] W. Scandale, R. Losito, E. Bagli, L. Bandiera, P. Dalpiaz, M. Fiorini, V. Guidi, A. Mazzolari, D. Vincenzi, G. D. Mea, E. Vallazza, A. Afonin, Y. Chesnokov, V. Maisheev, I. Yazynin, A. Kovalenko, A. Taratin, A. Denisov, Y. Gavrikov, Y. Ivanov, L. Lapina, V. Skorobogatov, D. Bolognini, S. Hasan, and M. Prest, *Physics Letters B* **719**, 70 (2013).

[13] A. Mazzolari, E. Bagli, L. Bandiera, V. Guidi, H. Backe, W. Lauth, V. Tikhomirov, A. Berra, D. Lietti, M. Prest, E. Vallazza, and D. De Salvador, *Phys. Rev. Lett.* **112**, 135503 (2014).

[14] A. Taratin and S. Vorobiev, *Physics Letters A* **119**, 425 (1987).

[15] W. Scandale, A. Vomiero, S. Baricordi, P. Dalpiaz, M. Fiorini, V. Guidi, A. Mazzolari, R. Milan, G. Della Mea, G. Ambrosi, B. Bertucci, W. J. Burger, M. Duranti, P. Zuccon, G. Cavoto, F. Iacoangeli, C. Luci, S. Pisano, R. Santacesaria, P. Valente, E. Vallazza, A. G. Afonin, Y. A. Chesnokov, V. I. Kotov, V. A. Maisheev, I. A. Yazynin, A. D. Kovalenko, A. M. Taratin, A. S. Denisov, Y. A. Gavrikov, Y. M. Ivanov, L. P. Lapina, L. G. Malyarenko, V. V. Skorobogatov, V. M. Suvorov, S. A. Vavilov, D. Bolognini, S. Hasan, D. Lietti, A. Mozzanica, and M. Prest, *Phys. Rev. Lett.* **101**, 234801 (2008).

[16] W. Scandale, A. Vomiero, E. Bagli, S. Baricordi, P. Dalpiaz, M. Fiorini, V. Guidi, A. Mazzolari, D. Vincenzi, R. Milan, G. D. Mea, E. Vallazza, A. G. Afonin, Y. A. Chesnokov, V. A. Maisheev, I. A. Yazynin, A. D. Kovalenko, A. M. Taratin, A. S. Denisov, Y. A. Gavrikov, Y. M. Ivanov, L. P. Lapina, L. G. Malyarenko, V. V. Skorobogatov, V. M. Suvorov, S. A. Vavilov, D. Bolognini, S. Hasan, A. Mattera, M. Prest, and V. V. Tikhomirov, *EPL (Europhysics Letters)* **93**, 56002 (2011).

[17] E. Bagli and V. Guidi, *Nuclear Instruments and Methods in Physics Research Section B: Beam Interactions with Materials and Atoms* **309**, 124 (2013).

[18] J. Lindhard, *Danske Vid. Selsk. Mat. Fys. Medd.* **34**, 14 (1965).

[19] E. Bagli, V. Guidi, and V. A. Maisheev, *Phys. Rev. E* **81**, 026708 (2010).

[20] J. Beringer, J. F. Arguin, R. M. Barnett, K. Copic, O. Dahl, D. E. Groom, C. J. Lin, J. Lys, H. Murrayama, C. G. Wohl, W. M. Yao, P. A. Zyla, C. Amssler, M. Antonelli, D. M. Asner, H. Baer, H. R. Band, T. Basaglia, C. W. Bauer, J. J. Beatty, V. I. Belousov, E. Bergren, G. Bernardi, W. Bertl, S. Bethke, H. Bichsel, O. Biebel, E. Blucher, S. Blusk, G. Brooijmans, O. Buchmueller, R. N. Cahn, M. Carena, A. Cecucci, D. Chakraborty, M. C. Chen, R. S. Chivukula, G. Cowan, G. D'Ambrosio, T. Damour, D. de Florian, A. de Gouv  a, T. DeGrand, P. de Jong, G. Dissertori, B. Dobrescu, M. Doser, M. Drees, D. A. Edwards, S. Eidelman, J. Erler, V. V. Ezhela, W. Fetscher, B. D. Fields, B. Foster, T. K. Gaisser, L. Garren, H. J. Gerber, G. Gerbier, T. Gherghetta, S. Golwala, M. Goodman, C. Grab, A. V. Gritsan, J. F. Grivaz, M. Grunewald, A. Gurtu, T. Gutsche, H. E. Haber, K. Hagiwara, C. Hagmann, C. Hanhart, S. Hashimoto, K. G. Hayes, M. Heffner, B. Heltsley, J. J. Hern  ndez-Rey, K. Hikasa, A. H  cker, J. Holder, A. Holtkamp, J. Huston, J. D. Jackson, K. F. Johnson, T. Junk, D. Karlen, D. Kirkby, S. R. Klein, E. Klemp, R. V. Kowalewski, F. Krauss, M. Kreps, B. Krusche, Y. V. Kuyanov, Y. Kwon, O. Lahav, J. Laiho, P. Langacker, A. Liddle, Z. Ligeti, T. M. Liss, L. Litten-

berg, K. S. Lugovsky, S. B. Lugovsky, T. Mannel, A. V. Manohar, W. J. Marciano, A. D. Martin, A. Massoni, J. Matthews, D. Milstead, R. Miquel, K. Mönig, F. Moortgat, K. Nakamura, M. Narain, P. Nason, S. Navas, M. Neubert, P. Nevski, Y. Nir, K. A. Olive, L. Pape, J. Parsons, C. Patrignani, J. A. Peacock, S. T. Petcov, A. Piepke, A. Pomarol, G. Punzi, A. Quadt, S. Raby, G. Raffelt, B. N. Ratcliff, P. Richardson, S. Roesler, S. Rolli, A. Romanouk, L. J. Rosenberg, J. L. Rosner, C. T. Sachrajda, Y. Sakai, G. P. Salam, S. Sarkar, F. Sauli, O. Schneider, K. Scholberg, D. Scott, W. G. Seligman, M. H. Shaevitz, S. R. Sharpe, M. Silari, T. Sjöstrand, P. Skands, J. G. Smith, G. F. Smoot, S. Spanier, H. Spieler, A. Stahl, T. Stanev, S. L. Stone, T. Sumiyoshi, M. J. Syphers, F. Takahashi, M. Tanabashi, J. Terning, M. Titov, N. P. Tkachenko, N. A. Törnqvist, D. Tovey, G. Valencia, K. van Bibber, G. Venanzoni, M. G. Vincter, P. Vogel, A. Vogt, W. Walkowiak, C. W. Walter, D. R. Ward, T. Watari, G. Weiglein, E. J. Weinberg, L. R. Wiencke, L. Wolfenstein, J. Womersley, C. L. Woody, R. L. Workman, A. Yamamoto, G. P. Zeller, O. V. Zenin, J. Zhang, R. Y. Zhu, G. Harper, V. S. Lugovsky, and P. Schaffner (Particle Data Group), Phys. Rev. D **86**, 010001 (2012).

[21] S. Agostinelli *et al.*, Nuclear Instruments and Methods in Physics Research Section A: Accelerators, Spectrometers, Detectors and Associated Equipment **506**, 250 (2003).

[22] Bagli, E., Asai, M., Brandt, D., Dotti, A., Guidi, V., and Wright, D. H., Eur. Phys. J. C **74**, 2996 (2014).

[23] G. Germogli, A. Mazzolari, L. Bandiera, E. Bagli, and V. Guidi, Nuclear Instruments and Methods in Physics Research Section B: Beam Interactions with Materials and Atoms **355**, 81 (2015).

[24] R. Camattari, V. Guidi, V. Bellucci, and A. Mazzolari, Journal of Applied Crystallography **48**, 977 (2015).

[25] J. Rosenzweig and L. Serafini, *The Physics of High Brightness Beams: Proceedings of the 2nd ICFA Advanced Accelerator Workshop* (World Scientific, 2000).

[26] K. Olive *et al.*, Chin. Phys. C **38**, 090001 (2014).

[27] A. Sørensen and E. Uggerhøj, (1989).

[28] E. Bagli, M. Asai, D. Brandt, A. Dotti, V. Guidi, and D. Wright, Eur. Phys. J. C **74**, 2996 (2014).

LaTeX Source Files

[Click here to download LaTeX Source Files: resubmission.zip](#)